Three-Dimensional Structure of κ-Conotoxin PVIIA, a Novel Potassium Channel-Blocking Toxin from Cone Snails[†,‡]

Philippe Savarin, Marc Guenneugues, Bernard Gilquin, Hung Lamthanh, Sylvaine Gasparini, Sophie Zinn-Justin,* and André Ménez*

CEA, Département d'Ingénierie et d'Études des Protéines, CE Saclay, 91191 Gif-sur-Yvette Cedex, France

Received December 10, 1997; Revised Manuscript Received February 3, 1998

ABSTRACT: κ-Conotoxin PVIIA from the venom of *Conus purpurascens* is the first cone snail toxin that was described to block potassium channels. We synthesized chemically this toxin and showed that its disulfide bridge pattern is similar to those of ω- and δ-conotoxins. κ-conotoxin competes with radioactive α-dendrotoxin for binding to rat brain synaptosomes, confirming its capacity to bind to potassium channels; however, it behaves as a weak competitor. The three-dimensional structure of κ-conotoxin PVIIA, as elucidated by NMR spectroscopy and molecular modeling, comprises two large parallel loops stabilized by a triple-stranded antiparallel β-sheet and three disulfide bridges. The overall fold of κ-conotoxin is similar to that of calcium channel-blocking ω-conotoxins but differs from those of potassium channel-blocking toxins from sea anemones, scorpions, and snakes. Local topographies of κ-conotoxin PVIIA that might account for its capacity to recognize Kv1-type potassium channels are discussed.

At least four groups of venomous animals produce toxins which block voltage-dependent potassium channels. These are the snakes, scorpions, sea anemones, and marine molluscs which synthesize well-known toxins, for example, α-dendrotoxin (*1*), charybdotoxin (*2*), BgK or ShK (*3*), and κ-conotoxin PVIIA (*4*), respectively. The mode of actions (*5*−*10*), three-dimensional structures (*11*−*14*), and functional topographies (*14*−*17*) of the first three types of toxins have been extensively investigated recently. These studies revealed that such toxins (i) compete with each other toward Kv1-type potassium channels; (ii) bind to the S5−S6 regions of the channel, definitive evidence existing for α-dendrotoxin (*18, 19*) and charybdotoxin (*20*) but not for BgK;[1] (iii) adopt unrelated architectures, despite their similar mode of actions; and (iv) possess functional topographies of about 700 Å^2, comprising approximately five critical residues. Moreover, each functional topography possesses a similar key diad, composed of a lysine and an hydrophobic residue (*14, 17*).

Thus, an unifying view is emerging which explains how toxins with unrelated structures can bind to various Kv1 potassium channels. It is proposed that an evolutionarily conserved minimal functional topography, reflected by the diad, might serve each toxin to bind to the Kv1 potassium channels, whereas the additional functional residues might provide the toxins with specific binding profiles toward one or various subtypes of Kv1 channels. To compare or modulate this view, the potassium channel-blocking toxins elaborated by the fourth group of venomous animals, i.e., the marine cone snails, need to be investigated. Little is known about the molecular properties of these toxins, referred to as κ-conotoxins. Do κ-conotoxins share the same three-dimensional structure and/or similar functional elements with any other potassium channel-blocking toxins from phylogenetically different animals? The present work is aimed at addressing these issues.

Cone snails produce a large diversity of functionally different toxins acting in particular on acetylcholine receptors, calcium channels, and sodium channels (*21, 22*). κ-Conotoxin PVIIA, which was isolated from the purple cone *Conus purpurascens*, acts in synergy with a toxin that delays inactivation of sodium channels and blocks the Shaker potassium channel with an EC_{50} of about 60 nM (*4*). It probably binds to the S5−S6 regions of voltage-dependent potassium channels (*23*). Its amino acid sequence contains 27 amino acids and 3 disulfide bonds. In the present paper, we report on (i) the chemical synthesis of κ-conotoxin PVIIA and the elucidation of its disulfide bond pattern; (ii) the competition of κ-conotoxin PVIIA with radioactive α-dendrotoxin toward rat brain synaptosomes, a material that includes Kv1-type potassium channels; and (iii) the three-dimensional structure of κ-conotoxin PVIIA, as calculated from ^{1}H NMR data. The results of our investigation reveal that the synthetic toxin binds to rat brain synaptosomes and adopts a three-dimensional structure that is similar to those of functionally unrelated toxins from cone shells but is different from those of potassium channel-blocking toxins found in snakes, sea anemones, and scorpions.

[†] M.G. was financially supported by IFSBM (Villejuif, France).

[‡] The atomic coordinates of the κ-conotoxin PVIIA have been deposited in the Brookhaven Protein Data Bank (file name 1KCP).

* Corresponding authors.

[1] Abbreviations: 2D, two dimensional; BgK, *Bunodosoma granulifera* K; BOP, benzotriazol-1-yloxytris(dimethylamino)phosphonium hexafluorophosphate; COSY, correlated spectroscopy; CTX, charybdotoxin; DIEA, diisopropylethylamine; DQF-COSY: double-quantum-filtered correlated spectroscopy; DTX, dendrotoxin; NMR, nuclear magnetic resonance; NOESY, nuclear Overhauser enhancement spectroscopy; rms, root mean square; TOCSY, total correlation spectroscopy; TCEP, tris(2-carboxyethyl)phosphine.

S0006-2960(97)03034-1 CCC: $15.00
Published on Web 03/26/1998

MATERIALS AND METHODS

Peptide Synthesis. κ-Conotoxin PVIIA was synthesized manually using the Fmoc strategy and a RINK amide resin with the BOP reagent as coupler (*24*). The Fmoc-peptide was deprotected and cleaved from the supporting resin with trifluoroacetic acid and purified on a C18 semipreparative column. The N-terminus was deprotected, and the material was purified before the folding step. The linear peptide was folded in the presence of reduced and oxidized glutathione as described (*25*). It was purified on a C18 semipreparative column and characterized by amino acid analysis, analytical HPLC, capillary electrophoresis, and electrospray mass spectrometry. The disulfide pattern was determined by partial reduction with TCEP and sequencing of the peptides (*26*).

Binding Assay. We evaluated the capacity of synthetic κ-conotoxin PVIIA to recognize potassium channels from rat brain synaptosomes by determining its capacity to compete with radioactive αDTX which predominantly recognizes Kv1 potassium channels (*27, 28*).

[^{125}I]αDTX was prepared by incubating 10 μg of synthetic αDTX at room temperature in a microtube (Eppendorf) coated with 1 μg of iodogen (Pierce) containing 2 mCi of iodine-125 (Amersham) in 200 μL of 0.1 M sodium phosphate. Fifteen minutes later, 20 μL of 0.1 M sodium thiosulfate was added, and the reaction mixture was injected onto a C18 column (Vydac). The column was washed with 25% solvent B (0.085% TFA, 50% acetonitrile) in solvent A (0.1% TFA) and then submitted to a 40 min gradient from 25% to 60% solvent B in solvent A (1 mL/min). The fraction containing pure monoiodinated αDTX (2000 Ci/mmol) was kept at 4 °C after addition of BSA (1 mg/mL). The binding ability of monoiodinated αDTX was determined by saturating 4 pM labeled toxin with increasing concentrations of rat brain synaptosomal membranes (0.35−24 μg of protein/mL). The yield was 84%. This value remained constant for at least 85 days.

Rat brain synaptosomal membranes were prepared as follows: ten rats (Sprague-Dawley) were killed with a guillotine. Decerebellate brains were homogenized in 100 mL of 10 mM Tris-HCl, pH 7.4, 10% sucrose, and 0.1 mM PMSF using successively an UltraTurrax T25 (IKA-Labortechnik) and a Potter. The whole homogenate was centrifuged at 1500*g* for 5 min, and the supernatant was recentrifuged for 10 min at 17000*g*. The pellet was resuspended in 80 mL of 5 mM Tris-HCl, pH 8, briefly homogenized with a glass Teflon homogenizer, and left for 2 h at 4 °C. Then, sucrose was added to the lysed membrane suspension at a final concentration of 36%. The suspension was centrifuged for 90 min at 28000 rpm using an SW28 rotor (Beckman) (66100−141000*g*) in tubes containing three layers of sucrose (36% (membrane suspension), 28.5%, and 10%). The synaptic membrane fraction (lower interface) was diluted to less than 10% sucrose in 10 mM Tris-HCl, pH 7.4, pelleted by centrifugation at 17000*g* for 10 min, washed twice with 10 mM Tris-HCl, pH 7.4, aliquoted, flash-frozen in liquid nitrogen, and stored at −80 °C. Protein concentration was determined by the method of Lowry using BSA as standard.

All competition binding experiments were done in 20 mM Tris-HCl, pH 7.4, 0.1 M NaCl, and 0.1% BSA in the presence of varying concentrations of unlabeled αDTX or κ-conotoxin. When equilibrium was reached, the incubation medium (1−5 mL) was rapidly filtered at room temperature through Whatman GF/C glass fiber filters that had been presoaked in 0.5% (w/v) polyethylenimine, followed by three washes with ice-cold filtration buffer (20 mM Tris-HCl and 0.15 M NaCl, 3 mL per wash). The radioactivity associated with the filters was then counted using a γ-counter.

Sample Preparation for NMR Study. The effects of temperature and pH on stability of κ-conotoxin were determined by monitoring the toxin circular dichroism spectrum using a JOBIN YVON CD6 spectrometer. No significant change was found between 190 and 240 nm at 293 K when the pH varied from 3.5 to 7.0. The peptide proved to be stable at 293 K and pH 3.5 over a period of at least 2 weeks. To be consistent with previous structural studies carried out for ω-conotoxins, our NMR experiments were recorded at 288 K and pH 5.0.

Five milligrams of κ-conotoxin was dissolved in 0.45 mL of solvent, such that the final concentration was 3.4 mM. The solvents used were either a mixture of 95% (v/v) H_2O and 5% (v/v) D_2O at pH 5.0 or 100% D_2O at pD 5.0. The pH (pD) was adjusted by addition of microliter amounts of dilute HCl (DCl). For the preparation of samples in D_2O, the amide protons were initially exchanged with deuterium by keeping the solution at 293 K for 7 days. Chemical shifts were referenced to internal 3-(trimethylsilyl)-[2,2,3,3-$^2H_4$]-propionate.

NMR Experiments. All NMR spectra were recorded between 275 and 308 K on a Bruker DRX500 spectrometer. The proton 2D experiments included COSY (*29*), DQF-COSY (*30*), TOCSY (*31*), and NOESY (*32*) experiments. Collection of angle and distance constraints was achieved on the basis of DQF-COSY and NOESY experiments, respectively, carried out in H_2O and D_2O at 288 K. NOESY spectra were recorded with a recycle time of 1.8 s and mixing times of 30, 50, 75, 100, and 150 ms. The water signal was suppressed by a WATERGATE sequence (*33*) except for the COSY experiments, where a low-power irradiation of the water frequency was used. All experiments were performed in the hypercomplex mode. The spectra were recorded with 512 $t_1 \times 1024$ t_2 points (1024 $t_1 \times 4096$ t_2 for the DQF-COSY). To study the slowly exchanging backbone amide protons, the sample was lyophilized and reconstituted in 99.96% D_2O. The residual NH signal was followed with time at 288 K by absolute value COSY experiments. One experiment was completed in 20 min. Spectra were recorded every 30 min during 28 h. Exchange rates were determined by fitting the COSY (NH, Hα) peak volume decay to a single exponential. The spectra were processed on a Silicon Graphics Indigo workstation (R8000) using UXNMR (Brüker) and Felix (*34*) programs.

Experimental Restraints. The volumes of the cross-peaks determined from NOESY spectra were integrated. For each peak, a buildup curve was constructed by fitting the experimental volumes to the following function of the mixing time: $f(\tau_m) = a\tau_m + b\tau_m^2$. The coefficient a was taken as the buildup rate of the corresponding NOE. Calibration of these dipolar correlation rates was achieved using a rigid body model of the protein, i.e., assuming that the buildup rates are proportional to r^{-6}. The buildup rates corresponding to geminal Hβ protons of about 10 residues were used as

references to calculate the coefficient of proportionality. We checked that the (NH, CH_α) distance values calculated with such a calibration were in the 2.2−3.5 Å range. The error made on the distances was evaluated as follows: for each proton pair, the root mean square deviation between the one, two, three, or four corresponding distances measured on both sides of the diagonal and in both solvents was calculated, and the root mean square deviations were plotted as a function of the distances. Thus, for 94% of the proton pairs, twice the root mean square deviation was found to be lower than 25% of the distance. We chose to apply an error of ±25% on the distance values for all proton pairs, except those for which twice the root mean square deviation was higher than 25% of the distance. For these proton pairs, an error equal to twice their root mean square deviation was used. Coupling constants were measured with a resolution of 0.9 Hz/point by evaluating the antiphase cross-peak separation on DQF-COSY spectra. ϕ angle restraints were derived from the $^3J_{HN-H\alpha}$ constants on the basis of the empirical Karplus relation (*35*); they were set to $-120° \pm 40°$ for $^3J_{HN-H\alpha} >$ 8 Hz, to $-120° \pm 60°$ for $^3J_{HN-H\alpha} = 5-8$ Hz when the intraresidue and sequential Hα−HN were clearly weak and strong, respectively, and to $-60° \pm 40°$ for $^3J_{HN-H\alpha} = 5-8$ Hz when the intraresidue or sequential Hα−HN were both weak. χ_1 angle values were determined using the method of Hyberts et al. (*36*). The boundaries of intervals were fixed to ±45°.

Structure Calculations. On the basis of suggestions from Dr. M. Nilges (*37*), we developed an automated iterative assignment procedure of the NOE buildup rates using the X-PLOR program (*38*) and C-shell routines. Assignment of κ-conotoxin PVIIA proton resonance frequencies showed that ^{1}H chemical shifts and $^3J_{HN-H\alpha}$ coupling constants are similar to those of ω-conotoxin MVIIC (*39*), allowing us to build by homology a model of the three-dimensional structure of κ-conotoxin PVIIA. Then, the NOE buildup rates were assigned on the basis of the proton chemical shift list and the predicted model. The rates which could not be assigned unambiguously were converted to ambiguous distance constraints (*40*). Only constraints consisting of less than four ambiguous possibilities were retained. Floating assignments for prochiral groups were used (*41*). On the basis of the resulting distance constraint list, 50 structures were generated. The 4 structures with lowest energy were selected in order to completely reassigned the NOE buildup list. The assignments were made on the basis of the chemical shift list and the averaged distance between protons in the 4 best structures. At each step of the procedure, 50 structures were generated and the 4 best structures were used to convert the NOE buildup list into a new distance constraint file. To increase the number of assigned NOE rates, the thresholds for both the chemical shift tolerance and the average maximum distance were increased from 0.012 to 0.025 ppm and from 5 to 6 Å, respectively. Ambiguous constraints were progressively assigned in keeping those corresponding to the closest distance. A force field adapted to NMR structure calculations (files topallhdg.pro and parallhdg.pro in X-PLOR 3.1) was used during the whole procedure.

After these iterations, several cross-peaks were still not assigned. To take into account the remaining protons which were separated by more than 6 Å and which, therefore, did not contribute to the assignment procedure, additional iterations were performed in which the distance threshold was set to 9 Å instead of 6 Å. At the end of this procedure, only 11 cross-peaks, which may correspond to a minor conformation, were not assigned. A total of 200 structures were calculated, and the 40 best ones (based on their energy value) were further refined. Restrained molecular dynamics at 600 K, slow cooling, and minimization were carried out with a standard energy function (files topallh22x.pro and parallh22x.pro in X-PLOR 3.1) comprising an electrostatic term. The electrostatic term was calculated with no net charge on the side-chain atoms and with a distance-dependent dielectric constant. The 22 structures being most consistent with the experimental data were selected for further analysis.

Comparison with Other Proteins Presenting the Same Fold. The structures of ω-conotoxin GVIA (*42, 43*), ω-conotoxin MVIIA (*44*), and ω-conotoxin MVIIC (*39*) were loaded from the Protein Data Bank, references 1OMC, 1CCO, 1OMG, and 1OMN, respectively.

RESULTS

Synthesis and Biological Properties

Synthesis of the κ-conotoxin PVIIA was carried out with a RINK amide resin (*45*), yielding a carboxamide form at the C-terminus, as usually observed for various members of the conotoxin family (*46*). Although an excess of 3 equiv in Fmoc-L-amino acid, BOP reagent, and DIEA was used for 1 h coupling, a recoupling step was necessary for Lys 19, Cys 15, Asp 13, Leu 12, His 11, Gln 10, Phe 9, and Cys 8. The synthetic κ-conotoxin PVIIA was obtained with an overall yield of 7.4% from the starting RINK amide resin. The purity of the peptide was assessed by RP-HPLC and capillary electrophoresis. The purified peptide displayed all expected chemical characteristics (not shown). In addition, its mass, as determined by electrospray mass spectrometry ($M_r = 3267.7$), agreed with that calculated for κ-conotoxin PVIIA ($M_r = 3267$).

κ-Conotoxin PVIIA possesses six half-cystines at positions 1, 8, 15, 16, 20, and 26. The pattern of its disulfide bonds was determined by reducing partially the disulfides (*26*) in order to generate intermediates in which some or all of the cystine bonds were reduced to cysteines. These intermediates were isolated by RP-HPLC, and the free cysteines were alkylated with an excess of iodoacetamide to give *S*-carboxamidomethyl (Cam) derivatives. Five major fractions eluted successively from the column and were submitted to sequencing. The first and the last fractions corresponded to fully oxidized and fully reduced κ-conotoxin PVIIA. The second fraction had two Cys(Cam) at cycles 1 and 16, indicating that Cys 1 and Cys 16 form a disulfide bond. The third fraction had Cys(Cam) at cycles 1, 15, 16, and 26. Since Cys 1 and Cys 16 were already known to be paired, Cys 15 and Cys 26 were concluded to constitute another disulfide bond. These data suggest that the third pair of disulfide bonds involves Cys 8 and Cys 20, in agreement with the analysis of the fourth fraction for which Cys(Cam) were found at cycles 1, 8, 16, and 20. Therefore, the disulfide pattern of κ-conotoxin can be unambiguously assigned to Cys 1−Cys 16, Cys 8−Cys 20, and Cys 15−Cys 26. Interestingly, this pairing is similar to that established for ω-conotoxins which act on calcium channels (*47*) and for δ-conotoxins which act on sodium channels (*48*). These data

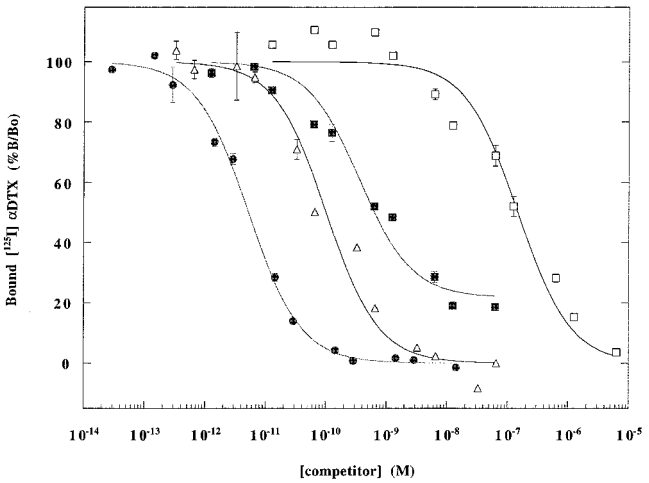

FIGURE 1: Inhibition of [^{125}I]αDTX binding to rat brain synaptosomal membranes by αDTX (closed circles), BgK (open triangles), charybdotoxin (closed squares), and κ-conotoxin PVIIA (open squares).

suggest that κ-conotoxin PVIIA adopts a fold similar to that of ω- and δ-conotoxins.

It was previously shown that, at a concentration 1 μM, κ-conotoxin PVIIA does not block cloned Kv1.1 and Kv1.4 channels from rat brain, although it blocks the cloned Shaker potassium channel with an EC_{50} of 60 $\pm$ 3 nM (at 0 mV) (*4*). We investigated the capacity of κ-conotoxin PVIIA to compete with [^{125}I]αDTX on rat brain synaptosomal membranes and compared it with the capacity of different potassium channel blockers from snakes, scorpions, and sea anemones to compete in the same assay. Figure 1 shows that unlabeled αDTX, CTX, BgK, and κ-conotoxin PVIIA all inhibit the binding of [^{125}I]αDTX to rat brain synaptosomes. αDTX, BgK, and κ-conotoxin PVIIA completely inhibited the binding of [^{125}I]αDTX whereas CTX inhibited only 80% of αDTX binding. The competition curves which fit to the experimental data were calculated by assuming that the toxins bind to a single class of sites. Thus, the four toxins clearly display different inhibitory potencies with K_i values equal to 3 $\pm$ 1 pM, 20 $\pm$ 8 pM, 120 $\pm$ 30 pM, and 50 $\pm$ 10 nM for αDTX, BgK, CTX, and κ-conotoxin PVIIA, respectively. Therefore, if κ-conotoxin inhibits the binding of iodinated αDTX, it also displays the lowest apparent affinity of all tested ligands. The αDTX-sensitive channels from rat brain form a heterogeneous family of molecules composed of Kv1-type subunits (*27*, *28*). Our data suggest that the affinities of κ-conotoxin PVIIA for the Kv1-type potassium channels present in rat brain are low. Nevertheless, the observed binding seems significant since, when tested under similar conditions and on the same target, the K_i values for ω-conotoxins MVIIA and MVIIC, described as calcium channel blockers (*49*, *50*), are 40- and 20-fold higher, respectively, than that of κ-conotoxin (not shown).

Structure Determination

Resonance Assignment. We investigated the three-dimensional structure of κ-conotoxin PVIIA in solution at pH 5.0 and 288 K by 2D ^{1}H NMR. Assignment of the chemical shifts was achieved for all nonlabile protons except H_ζ of Phe 9 and for all labile protons except the N-terminal ammonium protons, the $H_{\delta 1}$ of His 11, and the side-chain ammonium protons of Arg 18 and Arg 22. Thus, the hydroxyl protons of Hyp 4 and Ser 17 and the ammonium protons of Arg 2 were observed, suggesting their participation as proton donors in intramolecular hydrogen bonds.

Experimental Distances and Angle Restraints. A total of 818 and 403 buildup rates were measured in H_2O and D_2O, respectively. Of them, 222 and 93 were rejected because of a poor fit to the second-order polynomial; 23 and 10 others were also removed because they corresponded to large superpositions of cross-peaks. Therefore, 873 buildup rates were used to determine the structure. A total of 17 ϕ and 3 χ_1 dihedral angle restraints were added to the experimental data set. The automated procedure described above led simultaneously to the attribution of the distance restraints and to the determination of the three-dimensional structure of κ-conotoxin PVIIA. A total of 33 steps of this procedure were necessary to obtain a family of structures consistent with the experimental data. As both sides of the diagonal of the NOESY spectra were analyzed, and as NOESY spectra were recorded in both H_2O and D_2O, many pairs, triplets, or even quadruplets of buildup rates corresponded to the same proton pair. When assignments of several peaks were identical, only one distance restraint was generated. At the end of the procedure, 434 distance restraints were used. Of them, 368 were unambiguous restraints and 66 were ambiguous restraints. The unambiguous restraint list consists of 218 intraresidues (in which 38 correspond to fixed distances), 68 sequential, 35 medium-range, and 47 long-range restraints (Figure 2). The resulting number of restraints per residue was 16.8.

Structural Statistics. Forty structures were refined in the CHARMM22 force field. Twenty-two of the final models (Table 1) had no distance violation larger than 0.5 Å and no dihedral angle violation larger than 10°. These structures had an acceptable covalent geometry, as evidenced by the low root mean square deviation values for bond lengths, valence angles, and improper dihedral angles. The value of the van der Waals energy was small, ruling out unfavorable nonbonded contacts. The Ramachandran plot confirmed the good quality of the 22 structures. In general, Asn 5, Arg 18, and Asn 24 were found in the L region of the plot; they were sometimes present in the generously allowed or even disallowed (for Arg 18) regions next to the L region, because of the narrow form of the L region compared to the resolution of the structures. Asn 5, Cys 8, and Ser 17 were found once, twice, and once in the generously allowed regions, respectively. All other residues were found in the most favored (70.5%) or in the additionally allowed regions (22.3%) of the Ramachandran plot.

Backbone Structure. Superimposition of the backbones of the 22 structures is shown in Figure 3a. The conformation of the backbone (N, Cα, C atoms) is well-defined, the atomic rms deviation with respect to the mean coordinate positions being equal to 0.59 $\pm$ 0.14 Å.

The 22 solution structures of κ-conotoxin PVIIA comprise a (+2*x*,−1) β-sheet from Gln 6 to Cys 8 (β_1), Lys 19 to Asn 21 (β_2), and Asn 25 to Val 27 (β_3). The atomic rms deviation with respect to the mean coordinate positions was equal to 0.46 $\pm$ 0.10 Å for the backbone atoms of the β-sheet, indicating that this part of the structure is particularly well-defined. Five backbone−backbone hydrogen bonds connect the three strands of the β-sheet. These are Cys 8 NH−Asn

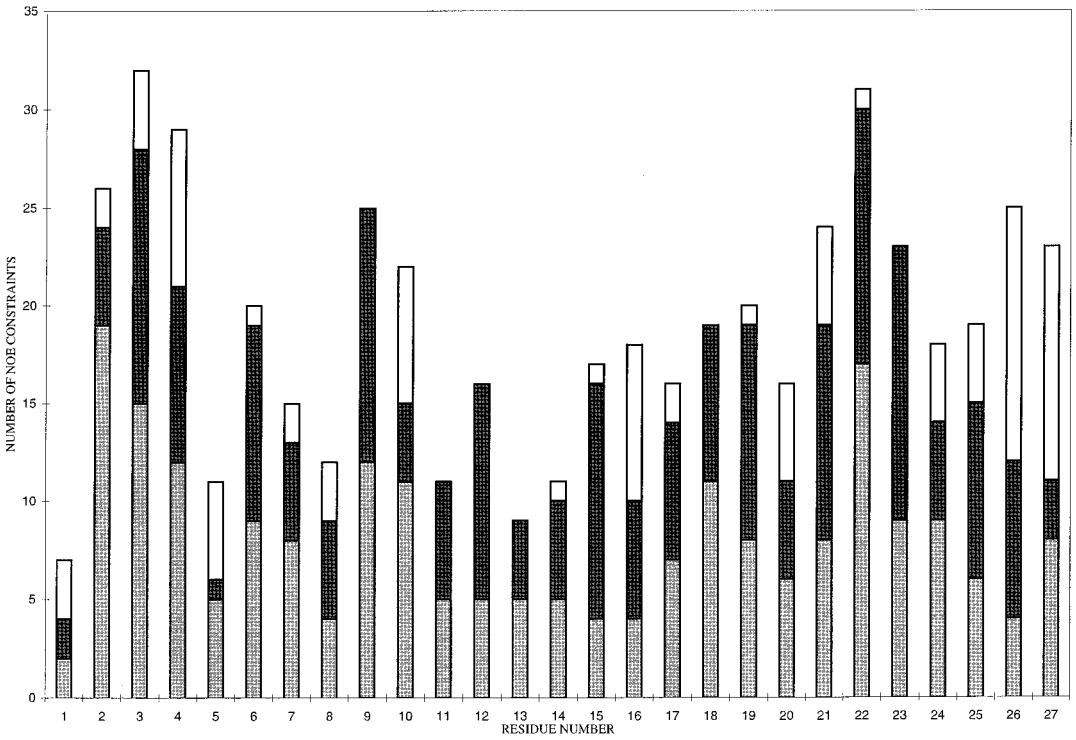

FIGURE 2: Plot versus the amino acid sequence of the number and the types of unambiguous NOE constraints per residue used in the calculation of the solution structure of κ-conotoxin PVIIA. The following code is used to define the different ranges of NOE constraints: in gray, intraresidue; in black, sequential and medium range; in white, long range.

Table 1: Structural Statistics[a]

rms differences from ideal values		
bond (Å)	0.0181	±0.0004
angle (deg)	3.4	±0.1
improper (deg)	2.7	±0.5
rms differences from restraints[b]		
distance (Å)	0.051	±0.005
dihedral angle (deg)	0.33	±0.05
energies (kcal/mol)[c]		
bond	−224.7	±17.9
angle	42.9	±2.2
improper	131.3	±6.2
electrostatic	−572.2	±15.8
vdW	3.0	±0.68
distance restraints	9.0	±9.7
dihedral angle restraints	23.6	±4.1
quality index[d]		
ϕ,ψ (%)	70.5	

[a] All values are averaged on the 22 X-PLOR structures. [b] The values of the square-well NOE and dihedral angle potentials are calculated with force constants of 20 kcal/(mol·Å^2) and 50 kcal/(mol·rad^2), respectively. [c] The van der Waals energy is calculated with a switch Lennard-Jones potential and CHARMM22 parameters (parallh22.pro). The electrostatic energy is calculated with a switch function, CHARMM22 parameters, no net charge on side-chain atoms, and a distance-dependent dielectric constant. [d] Percentage of residues in most favorable regions of the Ramachandran plot is calculated with Procheck-nmr (*62*).

24 O, Cys 26 NH−Gln 6 O, Asn 5 NH−Cys 26 O (noncanonical), Asn 21 NH−Lys 25 O, and Val 27 NH−Ser 19 O. They were present in more than 86% of the structures, and their corresponding amides were still observable after 20 min in D_2O.

The N-terminal region which precedes the β_1-strand is formed by Arg 2 and Ile 3, which adopt an extended conformation, followed by a type II β-turn from Ile 3 to Gln 6. The hydrogen bond that is characteristic of the β-turn was present in 95% of the structures, and the amide proton of Gln 6 was still observable after 20 min in D_2O.

The region linking the β_1- and β_2-strands is the less defined part of the structure. It is formed by residue Phe 9 in an extended conformation, followed by a type I β-turn from Phe 9 to Leu 12, a four-residue loop from Leu 12 to Cys 15, and a type I β-turn from Cys 15 to Arg 18. A hydrogen bond was observed in the loop, involving Asp 14 HN−Leu 12 O. It was present in half of the structures, and the corresponding amide was not observable after 20 min in D_2O. The hydrogen bonds that are characteristic of both β-turns were present in more than 77% of the structures, but only the amide proton of Arg 18 was still observable after 20 min in D_2O.

Finally, residues Asn 21−Asn 24 form a type I β-turn that links the β_2- and β_3- strands. The backbone−backbone hydrogen bond characteristic of the β-turn was present in 73% of the structures, and the amide proton of Asn 24 was still observable after 20 min in D_2O. An additional backbone−side-chain hydrogen bond stabilizes the conformation of the β-turn. It involves Phe 23 HN and Asn 21 $O_{\delta 1}$. It was present in 91% of the structures, and the amide of Phe 23 was still observable after 20 min in D_2O. A pseudobulge formed by Asn 21, Asn 24, and Lys 25 is observed between the β-turn and the β_2/β_3-sheet (*51*). This bulge is characterized by a backbone−backbone hydrogen bond, Asn 24 HN−Asn 21 O, which belongs also to the β-turn, and by a backbone−side-chain hydrogen bond, Lys 25 HN−Asn 21 $O_{\delta 1}$ that is found in almost half of the structures. Experimentally, the corresponding amide protons were still observable after 20 min in D_2O. The pseudobulge is close to a G1-type bulge, which is consistent with the nature of its amino acids (*52*).

Two hydrogen bonds are involved in the positioning of the N-terminal region relative to the loop Leu 12−Cys 15. These are Arg 2 HN−Asp 14 O and Cys 16 HN−Arg 2 O,

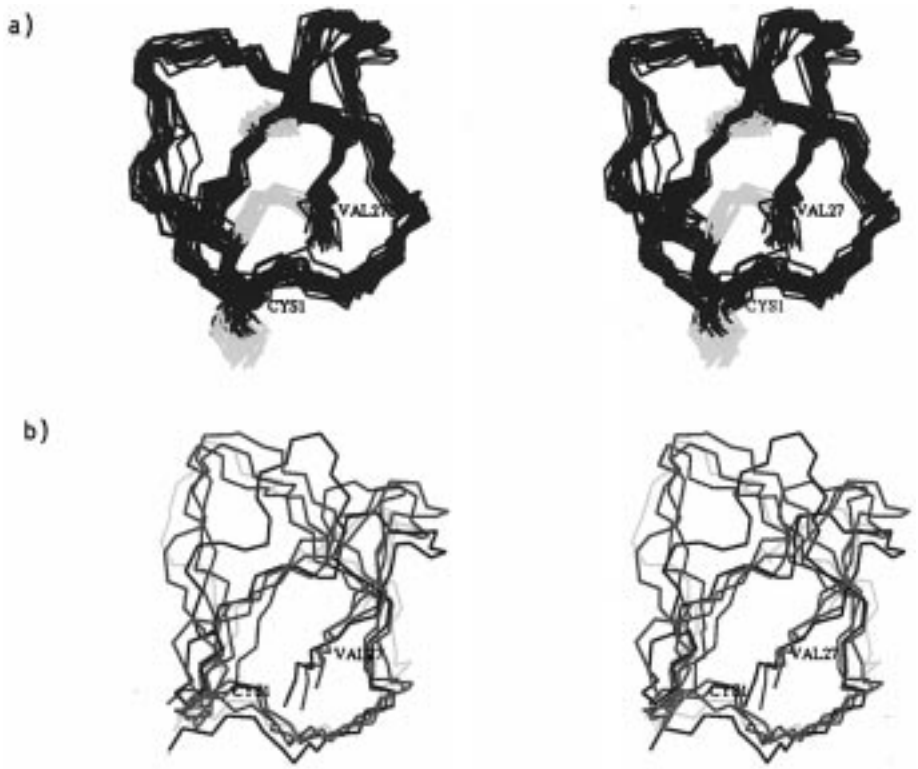

FIGURE 3: (a) Stereoview of the superimposition of the polypeptide backbone atoms of the 22 final solution structures of κ-conotoxin PVIIA (disulfide bridges are represented in yellow). (b) Stereoview of the best fit superimposition of κ-conotoxin PVIIA (in red) and ω-conotoxins GVIA [(*42*) in cyan; (*43*) in blue], MVIIA [(*44*), in purple], and MVIIC [(*39*) in yellow].

which were found in more than 68% of the structures. None of the corresponding amide protons could be observed after 20 min in D_2O.

Disulfide Bonds. The two most solvent accessible disulfide bridges (1−16 and 8−20) do not adopt unique and classical conformations. The core disulfide bridge (15−26), which is completely buried, adopts in most structures a common left-handed conformation. A characteristic of the κ-conotoxin PVIIA fold is that a ring is formed by the two disulfide bridges (1−16, 8−20) and the two segments of the interconnecting backbones (1−8, 16−20). The core disulfide bridge passes through this ring, thus forming a "disulfide knot".

Side Chains. When calculated on the heavy atoms, the atomic rms deviation with respect to the mean coordinate positions is equal to 1.36 ± 0.21 Å. Analysis of the side-chain orientations showed that 15 of the 26 χ_1 values are well determined; i.e., their circular variances are lower than 0.2. The best defined side chains, as judged by their rms deviation relative to the mean structure and their χ_1 distribution, correspond approximately to the buried side chains. Thus, the side chains that are more than half-buried in the structure all have an rmsd lower than 1.6 Å, except Arg 2 (rmsd = 1.98 Å), and all have a circular variance lower than 0.27, except Asn 24 (variance = 0.41).

These buried side chains correspond to residues Arg 2, Gln 6, Gln 10, Leu 12, Ser 17, Asn 21, Asn 24, and Lys 25 and the six cystines. The side chain of Gln 6 makes a hydrogen bond with the amide of Lys 7 in most of the structures. The side chain of Leu 12 interacts with those of Arg 2, Phe 9, His 11, and Asp 14. It participates to the spatial organization of the side chains of the N-terminal 16-residue loop. The side chain of Lys 25 makes numerous van der Waals contacts with Asn 5, Lys 7, Asn 21, and Phe 23. The presence of this important aliphatic side chain may be critical for the organization of the solvent-exposed side of the triple β-sheet. The side chain of Asn 21 interacts with the amides of Phe 23 and Lys 25 and hence may stabilize the β-turn and β-bulge structures in the Asn21−Lys 25 region. The side chain of Gln 10 makes hydrogen bonds with the carbonyl of Asn 21 in most of the structures and with the side chain of Asn 24 in almost half of the structures. These interactions may influence the positioning of the N-terminal 16-residue loop relative to the β-turn Asn 21−Asn 24.

The side chains of residues Arg 2, Hyp 4, and Ser 17 have slowly exchanging secondary amine or hydroxyl protons whose resonance frequencies could thus be attributed. These labile protons are involved in intramolecular hydrogen bonds. The secondary amines of Arg 2 are alternatively hydrogen bonded to carbonyls belonging to residues Lys 7 and Asp 14. Therefore, Arg 2 may play a central role in the positioning of the first 16 residues around its side chain. The hydroxyl proton of Hyp 4 is hydrogen bonded to the carbonyl of Val 27 in almost half of the structures. The hydroxyl of Ser 17 is hydrogen bonded to the same carbonyl in more than half of the structures. In fact, a network of backbone−side-chain hydrogen bonds stabilizes the interaction between the N-terminal 16-residue loop (Hyp 4, Ser 17) and the C-terminal β-strand (Val 27).

DISCUSSION

Initially, κ-conotoxin was discovered in the venom of *C. purpurascens* (*4*). In the present work, we have used a synthetic version of the toxin. However, recent evidence

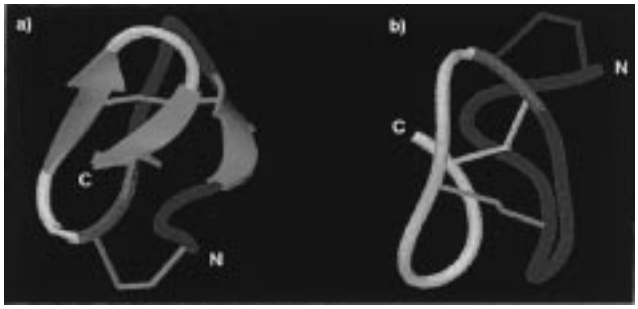

FIGURE 4: Ribbon representation of backbone atoms of the averaged mininized structure of κ-conotoxin PVIIA. The first loop is colored in dark blue and the second loop in yellow. The two cysteines belonging to both loops are colored in cyan. (a) The three-stranded β-sheet is represented by red arrows, and the three disulfide bridges are displayed in orange. (b) The disulfide bridge 1−16 connecting the N- and C-termini of the first loop is colored in dark blue, and the disulfide bridge 15−26 connecting the N- and C-termini of the second loop is colored in yellow. The disulfide bridge 8−20 connecting the two loops is in orange.

indicates that this material corresponds to the toxin that is present in the venom. First, the synthesis and folding steps were readily achieved with reasonable yields. Second, we determined that the three disulfide bonds are cystine 1−16, cystine 8−20, and cystine 15−26, a pattern that is similar to that of other cone snail toxins (*47*, *48*). Third, the three-dimensional structure of κ-conotoxin, as reported in this paper, is similar to those of other conotoxins (*42*−*44*, *53*−*57*). Fourth, it was reported that κ-conotoxin acts on potassium channels (*4*), and accordingly, we demonstrated that this peptide can inhibit the binding of radioactive α-dendrotoxin to rat brain membranes with a higher affinity as compared to other conotoxins adopting the same fold.

The three-dimensional structure of κ-conotoxin PVIIA consists of two large loops stabilized by a triple-stranded β-sheet and three disulfide bridges (Figure 4). The N-terminal loop spans from residue 1 to residue 16 and comprises the β-turn Ile 3−Gln 6, the β-strand Gln 6−Cys 8, and the β-turn Phe 9−Leu 12. The disulfide bridge (1−16) closes this loop, whereas the secondary amines of Arg 2 are localized at the center of the loop, establishing a network of hydrogen bonds with carbonyl oxygens of the loop backbone. A flat surface is defined by Arg 2 and its surrounding side chains. This surface is formed by various types of amino acids including positively (Arg 2, Lys 7) and negatively (Asp 14) charged residues, neutral and polar residues (Gln 6, His 11, Asn 24), and hydrophobic residues (Ile 3, Phe 9, Leu 12). The second loop lies from residue 15 to residue 27. It comprises the β-turn Cys 15−Arg 18, two antiparallel β-sheet strands, Lys 19−Asn 21 (β_2) and Asn 25−Val 27 (β_3), and the β-turn Asn 21−Asn 24. It is closed by the disulfide bridge Cys 15−Cys 26. Another flat surface can be defined around the side chains of the solvent-exposed side of the β_2/β_3 sheet. This surface contains positively charged amino acids (Lys 7, Lys 19, Arg 22, Lys 25), neutral and polar amino acids (Hyp 4, Asn 5, Ser 17, Asn 21), and hydrophobic amino acids (Phe 23, Val 27). The planes defined by the two large loops, 1−16 and 15−27, are almost parallel (Figure 4b). The positioning of the two loops is stabilized by the third disulfide bridge, Cys 8−Cys 20, as well as by numerous backbone and side-chain/side-chain interactions (Gln 10/Asn 21 and Asn 24; Lys 25/Asn 5 and Lys 7; Hyp 4 and Ser 17/Val 27).

The primary structures of κ-conotoxin PVIIA and ω-conotoxins GVIA, MVIIA, and MVIIC share few analogies (Figure 5). If one excludes the half-cystines, the ω-conotoxins share only two to four residues with κ-conotoxin PVIIA. Nevertheless, the HN and Hα chemical shifts and the $^3J_{HN-H\alpha}$ coupling constants of κ-conotoxin PVIIA are highly similar to those of ω-conotoxins GVIA, MVIIA, and MVIIC. As an illustration, Figure 6 shows a comparison of the chemical shifts and coupling constants of κ-conotoxin PVIIA and ω-conotoxin MVIIC (*39*): only five HN and six Hα have chemical shifts separated by more than 0.3 and 0.6 ppm, respectively; most of the $^3J_{HN-H\alpha}$ coupling constants are identical within their experimental errors. Consistently, the positions in the sequence of the triple β-sheet and the four β-turns, as well as the types of turns, sequentially characterized as II, I, I or VIII, and I or I′ according to Wilmot and Thornton (*58*), are conserved in both κ- and ω-conotoxins (*39*, *42*−*44*, *53*−*57*). Altogether, these data clearly show that κ- and ω-conotoxins adopt a similar fold.

Figure 3b shows how nicely the backbone of κ-conotoxin PVIIA superimposes with those of ω-conotoxins GVIA, MVIIA, and MVIIC. All these structures are very close to each other, the atomic rms deviations between κ-conotoxin PVIIA and ω-conotoxins GVIA, MVIIA, and MVIIC being 0.93 ± 0.07, 1.46 ± 0.1, and 1.58 ± 0.24 Å, respectively. For the backbone atoms of the three-stranded β-sheet, the atomic rms deviation between κ-conotoxin PVIIA and these toxins is 0.52 ± 0.04, 0.73 ± 0.07, and 1.03 ± 0.11 Å, respectively, which indicates that the structure of the three-stranded β-sheet is particularly well conserved. Insertions or deletions that occur in the different toxins can be readily accommodated within the conserved fold by changing the number of residues between the third turn and the β_2-strand and by placing a bulge between the β_2/β_3-sheet and the fourth turn. The three disulfide bridges adopt the same preferential conformation in all the toxins. Several residues of the protein core, i.e., Ser 17, Asn 21, and Lys 25, show as do the cystine residues a low solvent accessibility and are conserved in at least one of the toxins. The side chains of these residues present the same orientation in all the toxins when the mutation is conservative.

Therefore, different cone snail toxins may adopt the same fold although they exert unrelated biological functions. Such a situation has already been encountered in other venomous animals, including snakes and scorpions (*59*, *60*), and perhaps corresponds to a general evolutionary strategy that allows venomous animals to respond to ecological changes.

The fold adopted by κ-conotoxin PVIIA is unrelated to any of the three other folds of toxins from scorpions (*12*), sea anemones (*13*, *14*), and snakes (*11*) that block Kv1 potassium channels. That a fourth fold is associated with a potassium channel-blocking activity further supports the previous proposal (*14*) that a convergent evolution might be associated with expression of a similar type of activity by toxins from phylogenetically distinct animals. In this respect, an even more precise functional organization was previously reported (*14*, *17*). Thus, the potassium channel-blocking toxins from snakes, scorpions, and sea anemones all possess a functionally important diad, consisting of a protruding key lysine and a hydrophobic residue, assisted by approximatively three additional residues. This organization offers an explanation for the functional similarities and differences

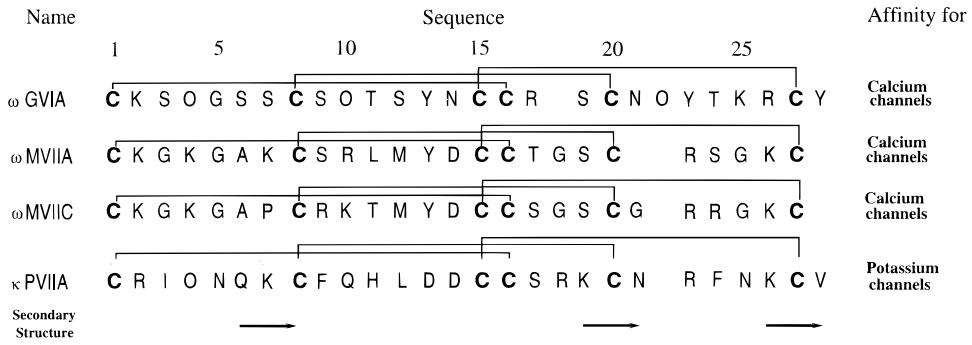

FIGURE 5: Alignment of the sequence of κ-conotoxin PVIIA with those of ω-conotoxins GVIA, MVIIA, and MVIIC. O represents a 4-*trans*-hydroxyproline.

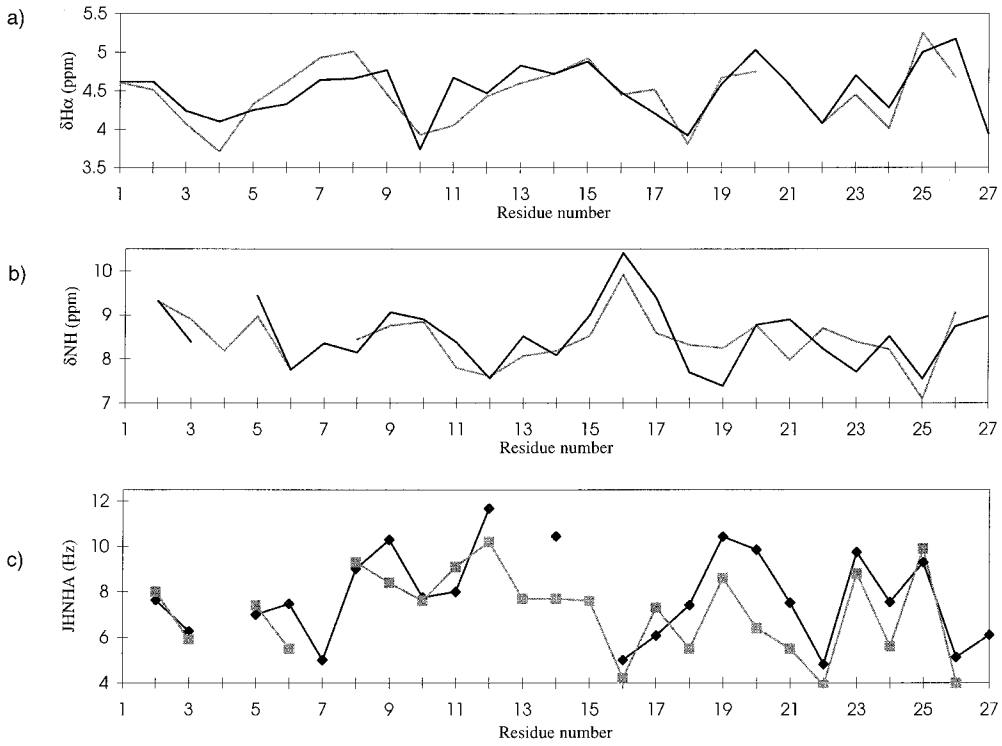

FIGURE 6: Comparison of the (a) HN and (b) Hα chemical shifts (in ppm) and (c) $^3J_{HN-H\alpha}$ coupling constants (in Hz) of κ-conotoxin PVIIA (gray) and of ω-conotoxin MVIIC (black) (*39*).

exerted by potassium channel-blocking toxins acting on Kv1 channels. The diad might serve the toxins to commonly anchor Kv1 channels whereas the additional functional residues might provide the toxins with various affinity and specificity profiles toward one or more potassium channel subtypes (Kv1.1, Kv1.2, Kv1.3, etc.). It was of interest, therefore, to examine whether κ-conotoxin PVIIA could display a similar type of surface organization. Three lysines, located at positions 7, 19, and 25, are present in κ-conotoxin PVIIA (Figure 7). If, by analogy with what has been found for scorpion toxins, we suppose that κ-conotoxin PVIIA blocks potassium channels by positioning a lysine into the vestibule of the channel pore (*9*), then at least one of the three lysines is critical for the activity of κ-conotoxin PVIIA. Lys 25 does not seem to be a favorable candidate because (i) it is present in functionally unrelated ω-conotoxins and (ii) its side chain is poorly solvent exposed, in contrast to key lysines of other potassium channel-blocking toxins. Lys 19 could be an interesting candidate, but it is close to the two negatively charged residues of the toxin, Asp 13 and Asp 14. At present, the critical lysine of potassium channel blockers has never been found close to a cluster of negative charges. Lys 7 is largely exposed to the solvent. Its side chain makes van der Waals contacts with the side chain of Lys 25 (Figure 7). A functional configuration involving two spatially close lysines has already been found in dendrotoxin K (*61*). Moreover, Lys 7 is rather close to two phenylalanines (Phe 9 and Phe 23). Together, Lys 7 and one of the phenylalanines could mimic the diad that is functionally important in other potassium channel-blocking toxins (*14*). Of course, in the absence of experimental evidence, one should consider these proposals with extreme care, especially because the affinity of κ-conotoxin PVIIA for Kv1 potassium channels is substantially lower than that of other potassium channel-blocking toxins from snakes, scorpions, and anemones. However, the knowledge of the structure of κ-conotoxin PVIIA offers an appropriate basis to search for the functional topography of this novel toxin. Considering the relatively small size of the κ-conotoxin PVIIA, it should be relatively easy to proceed to a systematic substitution of the different residues of its amino acid sequence and hence to identify the functionally critical residues.

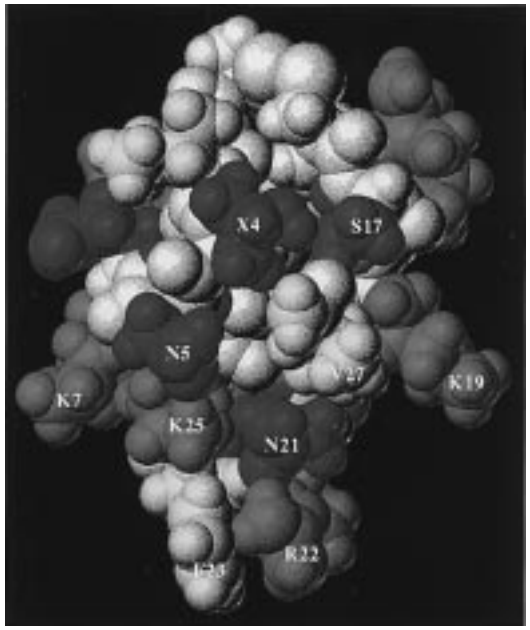

FIGURE 7: Space-filling view of the solvent-exposed side chains of the three-stranded β-sheet of κ-conotoxin PVIIA. Positively charged, neutral and polar, and hydrophobic side chains are colored in cyan, green, and yellow, respectively.

NOTE ADDED IN PROOF

While this paper was being reviewed, a communication was published (*63*) with the definitive sequence of κ-conotoxin PVIIA. In this communication, it is clearly stated that the C-terminus of κ-conotoxin PVIIA is not amidated. Furthermore, a second communication was published (*64*) with the solution structure of κ-conotoxin PVIIA containing a nonamidated C-terminus. This structure is apparently very similar to ours, suggesting that the C-terminal amidation does not provoke any important structural change in κ-conotoxin PVIIA. Interestingly, the discussion of the toxin structure in this second communication leads to conclusions quite different from ours.

SUPPORTING INFORMATION AVAILABLE

One table listing proton resonance chemical shifts (in ppm) of κ-conotoxin PVIIA at 288 K and pH 5.0 (1 page). Ordering information is given on any current masthead page.

REFERENCES

1. Harvey, A. L., and Karlsson, E. (1980) *Naunyn-Scmiedeberg's Arch. Pharmacol. 28*, 231−253.
2. Gimenez-Gallego, G., Navia, M. A., Reuben, J. P., Katz, G. M., Kaczorwski, G. J., and Garcia, M. L. (1988) *Proc. Natl. Acad. Sci. U.S.A. 85*, 3329−3333.
3. Aneiros, A., Garcia, I., Martinez, J. R., Harvey, A. L., Anderson, A. J., Marshall, D. L., Engström, A., Hellman, U., and Karlsson, E. (1993) *Biochim. Biophys. Acta 1157*, 86−92.
4. Terlau, H., Shon, K.-J., Grilley, M., Stocker, M., Stühmer, W., and Olivera, B. M. (1996) *Nature 381*, 148−151.
5. Harvey, A. L. (1993) *Med. Res. Rev. 13*, 81−104.
6. Harvey, A. L. (1997) *Gen. Pharmacol. 28*, 7−12.
7. Harvey, A. L., and Anderson, A. J. (1991) in *Snake Toxins* (Harvey, A. L., Ed.) pp 131−164, Pergamon Press, New York.
8. Dolly, J. O., and Parcej, D. N. (1996) *J. Bioenerg. Biomembr. 28*, 231−253.
9. Miller, C. (1995) *Neuron 15*, 5−10.
10. Cotton, J., Crest, M., Bouet, F., Alessandri, N., Gola, M., Forest, E., Karlsson, E., Castaneda, O., Harvey, A. L., Vita, C., and Ménez, A. (1997) *Eur. J. Biochem. 244*, 192−202.
11. Skarzynski, T. (1992) *J. Mol. Biol. 224*, 671−683.
12. Bontems, F., Roumestand, C., Gilquin, B., Ménez, A., and Toma, F. (1991) *Science 254*, 1521−1523.
13. Tudor, J. E., Pallaghy, P. K., Pennington, M. W., and Norton, R. S. (1996) *Nat. Struct. Biol. 3*, 317−320.
14. Dauplais, M., Lecoq, A., Song, J., Cotton, J., Jamin, N., Gilquin, B., Roumestand, C., Vita, C., de Medeiros, C. L. C., Rowan, E. G., Harvey, A. L., and Ménez, A. (1997) *J. Biol. Chem. 272*, 4302−4309.
15. Goldstein, S. A., and Miller, C. (1993) *Neuron 12*, 1377−1388.
16. Pennington, M. W., Manhir, V. M., Khaytin, I., Zaydenberg, I., Byrnes, M. E., and Kem, W. R. (1996) *Biochemistry 35*, 16407−16411.
17. Gasparini, S., Danse, J.-M., Lecoq, A., Pinkasfeld, S., Zinn-Justin, S., Young, L. C., de Medeiros, C. C. L., Rowan, E. G., Harvey, A., and Ménez, A. *J. Biol. Chem.* (submitted for publication).
18. Hurst, R. S., Busch, A. E., Kavanaugh, M. P., Osborne, P. B., North, R. A., and Adelman, J. P. (1991) *Mol. Pharmacol. 40*, 572−576.
19. Stocker, M., Pongs, O., Hoth, M., Heinemenn, S. H., Stühmer, W., Schröter, K.-H., and Ruppersberg, J. P. (1991) *Proc. R. Soc. London B 245*, 101−107.
20. Gross, A., Abramson, T., and MacKinnon, R. (1994) *Neuron 13*, 961−966.
21. Olivera, B. M., Gray, W. R., Zeikus, R., McIntosh, J. M., Varga, J., Rivier, J., De Santos, V., and Cruz, L. (1985) *Science 230*, 1338−1343.
22. Adams, M. E., and Olivera, B. M. (1994) *Trends Neurosci. 17*, 151−155.
23. Kim, M., Baro, D. J., Lanning, C. C., Doshi, M., Farnham, J., Moskowitz, H. S., Peck, J. H., Olivera, B. M., and Harris-Warrick, R. M. (1997) *J. Neurosci. 17*, 8213−8224.
24. Castro, B., Dormoy, J. R., Evin, G., and Selve, C. (1975) *Tetrahedron Lett. 14*, 1219−1222.
25. Kubo, S., Chino, N., Kimura, T., and Sakakibara, S. (1996) *Biopolymers 38*, 733−744.
26. Gray, W. R. (1993) *Protein Sci. 2*, 1732−1748.
27. Scott, V. S. E., Muniz, Z. M., Sewing, S., Lichtinghagen, R., Parcej, D. N., Pongs, O., and Dolly, O. (1994) *Biochemistry 33*, 1617−1623.
28. Shamotienko, O., Parcej, D. N., and Dolly, J. O. (1997) *Biochemistry 36*, 8195−8201.
29. Aue, W. P., Bartholi, E., and Ernst, R. R. (1976) *J. Chem. Phys. 64*, 2229−2246.
30. Rance, M., Sorensen, O., Bodenhausen, G., Wagner, G., Ernst, R. R., and Wüthrich, K. (1983) *Biochem. Biophys. Res. Commun. 117*, 479−485.
31. Braunschweiler, L., and Ernst, R. R. (1983) *J. Magn. Reson. 53*, 521−528
32. Kumar, A., Ernst, R. R., and Wühtrich, K. (1980) *Biochem. Biophys. Res. Commun. 95*, 1−6.
33. Piotto, M., Saudek, V., and Sklenar, V. (1992) *J. Biomol. NMR 2*, 661−665.
34. Biosym Technologies (1995) *FELIX Software*, San Diego, CA.
35. Pardi, A., Billeter, M., and Wühtrich, K. (1984) *J. Mol. Biol. 180*, 740−751.
36. Hyberts, S. G., Märki, W., and Wagner, G. (1987) *Eur. J. Biochem. 164*, 625−635.
37. Nilges, M., Macias, M. J., O'Donoghue, S. I., and Oschkinat, H. (1997) *J. Mol. Biol. 269*, 408−422.
38. Brünger, A. T. (1992) *X-PLOR Version 3.1: A System for X-ray Crystallography and NMR*, Yale University Press, New Haven and London.
39. Farr-Jones, S., Miljanich, G. P., Nadasdi, L., Ramachandran, J., and Basus, V. J. (1995) *J. Mol. Biol. 248*, 106−124.
40. Nilges, M. (1995) *J. Mol. Biol. 245*, 645−660.
41. Folmer, R. H., Hilbers, C. W., Konings, R. N., and Nilges, M. (1997) *J. Biomol. NMR 9*, 245−258.

42. Davis, J. H., Bradley, E. K., Miljanich, G. P., Nadasdi, L., Ramachandran, J., and Basus, V. J. (1993) *Biochemistry 32*, 7396−7405.
43. Pallaghy, P. K., Duggan, B. M., Pennington, M. W., and Norton, R. S. (1993) *J. Mol. Biol. 234*, 405−420.
44. Kohno, T., Kim, J. I., Kobayashi, K., Kodera, Y., Maeda, T., and Sato, K. (1995) *Biochemistry 34*, 10256−10265.
45. Rink, H. (1987) *Tetrahedron Lett. 28*, 3787−3790.
46. Myers, R. A., Cruz, L. J., Rivier, J. E., and Olivera, B. M. (1993) *Chem. Rev. 93*, 1923−1936.
47. Olivera, B. M., Miljanich, G. P., Ramachandran, J., and Adams, M. E. (1994) *Annu. Rev. Biochem. 63*, 823−867.
48. Shon, K.-J., Hasson, A., Spira, M. E., Cruz, L. J., Gray, W. R., and Olivera, B. M. (1994) *Biochemistry 33*, 11420−11425.
49. Olivera, B. M., Cruz, L. J., de Santos, V., LeCheminant, G. W., Griffin, D., Zeikus, R., McIntosh, J. M., Galyean, R., Varga, J., and Gray, W. R. (1987) *Biochemistry 26*, 2086−2090.
50. Wheeler, D. B., Randall, A., and Tsien, R. W. (1994) *Science 264*, 107−111.
51. Richardson, J. S., Getzoff, E. D., and Richardson, D. C. (1978) *Proc. Natl. Acad. Sci. U.S.A. 75*, 2574−2578.
52. Chan, A. W., Hutchinson, E. G., Harris, D., and Thornton, J. M. (1993) *Protein Sci. 2*, 1574−1590.
53. Sevilla, P., Bruix, M., Santoro, J., Gago, F., Garcia, A. G., and Rico, M. (1993) *Biochem. Biophys. Res. Commun. 3*, 1238−1244.
54. Skalicky, J. J., Metzler, W. J., Ciesla, D. J., Galdes, A., and Pardi, A. (1993) *Protein Sci. 2*, 1591−1603.
55. Basus, V. J., Nadasdi, L., Ramachandran, J., and Miljanich, G. P. (1995) *FEBS Lett. 21*, 163−169.
56. Nemoto, N., Kubo, S., Yoshida, T., Chino, N., Kimura, T., Sakakibara, S., Kyogoku, Y., and Kobayashi, Y. (1995) *Biochem. Biophys. Res. Commun. 207*, 695−699.
57. Nielsen, K. J., Thomas, L., Lewis, R. J., Alewood, P. F., and Craik, D. J. (1996) *J. Mol. Biol. 263*, 297−310.
58. Wilmot, C. M., and Thornton, J. M. (1990) *Protein Eng. 3*, 479−493.
59. Ménez, A., Bontems, F., Gilquin, B., and Toma, F. (1992) *Proc. R. Soc. Edinburgh 99B*, 83−103.
60. Ménez, A., and Dauplais, M. (1997) *Sci. Spectra 8*, 44−50.
61. Smith, L., Reid, P. F., Wang, F. C., Parcej, D. N., Schmidt, J. J., Olson, M. A., and Dolly, J. O. (1997) *Biochemistry 36*, 7690−7696.
62. Laskowski, R. A., Rullmann, A. C., MacArthur, M. W., Kaptein, R., and Thornton, J. M. (1996) *J. Biomol. NMR 8*, 477−486.
63. Shon, K.-J., Stocker, M., Terlau, H., Stühmer, W., Jacobsen, R., Walker, C., Grilley, M., Watkins, M., Hillyard, D. R., Gray, W. R., and Olivera, B. M. (1998) *J. Biol. Chem. 273*, 33−38.
64. Scanlon, M. J., Naranjo, D., Thomas, L., Alewood, P. F., Lewis, R. J., and Craik, D. J. (1997) *Structure 5*, 1585−1597.

BI9730341